Supporting Information (SI)

Hydrodeoxygenation of Guaiacol over Bimetallic Fe-Alloyed (Ni, Pt) Surfaces: Reaction Mechanism, Transition-State Scaling Relations and Descriptor for Predicting C-O Bond Scission Reactivity

Xiaoyang Liu[a], Wei An[a]*, Yixing Wang[a], C. Heath Turner[b], Daniel E. Resasco[c]

[a]College of Chemistry and Chemical Engineering, Shanghai University of Engineering Science, Songjiang District, Shanghai 201620, China

[b]Department of Chemical and Biological Engineering, University of Alabama, Tuscaloosa, AL 35487-0203, United States

[c]School of Chemical, Biological and Materials Engineering and Center for Biomass Refining, University of Oklahoma, Norman, OK 73019, United States

*E-mail: weian@sues.edu.cn

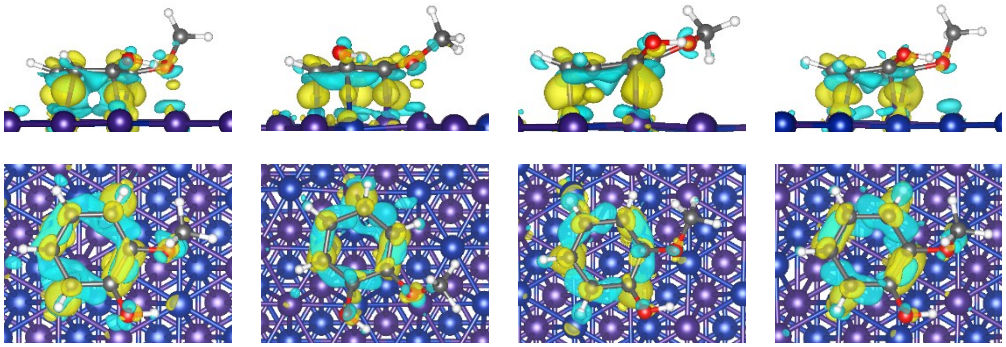

Figure S1. Side view (top) and top view (bottom) of three-dimensional charge density difference isosurfaces for four hcp/fcc sites of guaiacol adsorbed on NiFe (111). Deep blue: Ni, purple: Fe, deep gray: C, black: H, red: O. The isovalue of isosurfaces: 0.004 e/Bohr^3, yellow isosurfaces: gain of electron density, cyan isosurfaces: loss of electron density.

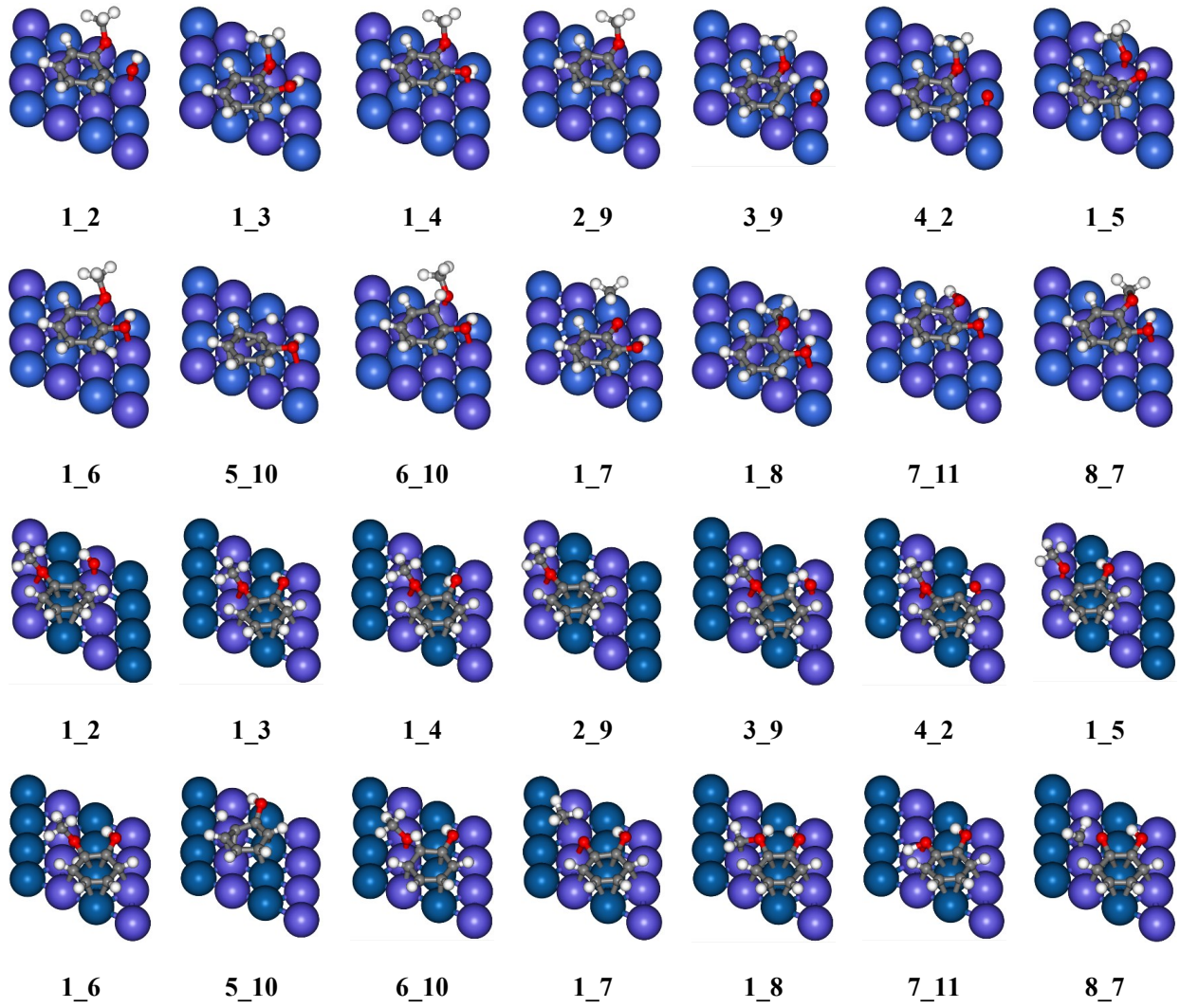

Figure S2. Optimized structures of transitions states (**n_m**) of elementary steps on (a) NiFe(111) and (b) PtFe(111) discussed in Section 3.2, where n and m represent initial state and final state, respectively, displayed in Figure 1. The numbers in italic denote activation barrier (in eV).

Table S1. C-O bond length (in Å) and binding energy (*BE*, in eV) of guaiacol at different adsorption sites on NiFe(111) and PtFe(111).

		hcp1/fcc1	hcp1/fcc2	hcp2/fcc1	hcp2/fcc2	gas-phase
NiFe(111)	C1-O1	1.39	1.38	1.39	1.38	1.37
	C2-O2	1.41	1.42	1.37	1.41	1.38
	C7-O2	1.46	1.45	1.44	1.45	1.43
	BE	**-1.82**	-1.30	-1.45	-1.19	
PtFe(111)	C1-O1	1.36	1.42	1.35	1.37	
	C2-O2	1.41	1.42	1.42	1.41	
	C7-O2	1.45	1.44	1.45	1.45	
	BE	**-1.39**	-1.22	-1.16	-1.14	

Table S2. Reaction energy (E_{rxn}) and activation barrier (E_a) with ZPE-correction for deoxygenation of guaiacol on NiFe(111) and PtFe(111).

Type	Reaction	NiFe(111)		PtFe(111)	
		E_{rxn}	E_a	E_{rxn}	E_a
C-O scission	**1** $C_6H_4(OH)(OCH_3) \rightarrow$ **2** $C_6H_4(OCH_3) + OH$	-0.16	1.42	0.57	2.05
	1 $C_6H_4(OH)(OCH_3) \rightarrow$ **5** $C_6H_4(OH) + OCH_3$	-0.29	1.37	0.25	1.97
	1 $C_6H_4(OH)(OCH_3) \rightarrow$ **7** $C_6H_4(OH)(O) + CH_3$	-0.77	0.91	-0.60	1.51
	3 $C_6H_4H_\alpha(OH)(OCH_3) \rightarrow$ **9** $C_6H_5(OCH_3) + OH$	-1.27	0.84	-1.09	0.76
	4 $C_6H_4(O)(OCH_3) \rightarrow$ **2** $C_6H_4(OCH_3) + O$	-0.22	1.80	0.44	1.87
	6 $C_6H_4H_\beta(OH)(OCH_3) \rightarrow$ **10** $C_6H_5(OH) + OCH_3$	-1.14	0.91	-1.05	0.91
	8 $C_6H_4(OH)(OCH_2) \rightarrow$ **7** $C_6H_4(OH)(O) + CH_2$	-0.71	0.54	-0.94	0.69
C-H formation	**1** $C_6H_4(OH)(OCH_3) + H \rightarrow$ **3** $C_6H_4H_\alpha(OH)(OCH_3)$	0.52	1.51	0.58	1.19
	1 $C_6H_4(OH)(OCH_3) + H \rightarrow$ **6** $C_6H_4H_\beta(OH)(OCH_3)$	0.56	1.54	0.60	1.08
	2 $C_6H_4(OCH_3) + H \rightarrow$ **9** $C_6H_5(OCH_3)$	-0.40	0.55	-1.47	0.37
	5 $C_6H_4(OH) + H \rightarrow$ **10** $C_6H_5(OH)$	-0.53	0.46	0.07	0.41
C-H scission	**1** $C_6H_4(OH)(OCH_3) \rightarrow$ **8** $C_6H_4(OH)(OCH_2) + H$	0.22	0.77	0.16	0.68
O-H scission	**1** $C_6H_4(OH)(OCH_3) \rightarrow$ **4** $C_6H_4(O)(OCH_3) + H$	-0.72	0.50	0.13	0.85
O-H formation	**7** $C_6H_4(OH)(O) + H \rightarrow$ **11** $C_6H_4(OH)_2$	0.51	1.26	0.28	0.93

Table S3 Binding energy (*BE*, in eV) of initial state (BE_{IS}), transition state (BE_{TS}) and final state (BE_{FS}) for two types of reactions (a) and (c): C-H bond formation (black line), (b) and (d): O-H bond scission (blue line), as shown in Figure 9. (A) Monometallic surfaces, (B) Bimetallic surfaces.

(A) Monometallic surfaces

Type	Ni(111)		Pt(111)		Ru(0001)		Pt(111)-p	
	BE_{IS}	BE_{TS}	BE_{IS}	BE_{TS}	BE_{IS}	BE_{TS}	BE_{IS}	BE_{TS}
(a) C-H formation	-5.06	-4.24	-2.98	-1.94	-4.40	-3.50	-2.26	-1.11
	-2.62	-1.94	-2.76	-1.76	-3.67	-2.83	-1.58	-0.59
	-4.95	-3.76	-2.64	-1.68	-3.41	-2.63	-1.34	-0.36
	-5.18	-4.38	-2.61	-1.50	-3.10	-2.17	-1.15	-0.15
			-3.15	-2.35	-5.41	-4.58	-0.90	0.06
							-2.44	-1.33
							-2.18	-1.15
							-1.93	-1.04
							-1.66	-0.72
							-1.29	-0.34
							-1.10	-0.27
	BE_{FS}	BE_{TS}	BE_{FS}	BE_{TS}	BE_{FS}	BE_{TS}	BE_{FS}	BE_{TS}
(b) O-H scission	-5.18	-4.42	-3.15	-2.97	-5.41	-4.02	-2.26	-1.97
	-2.93	-2.44					-1.58	-1.32
	-4.47	-3.94					-1.42	-1.14
	-5.41	-4.71					-1.41	-0.90
							-0.89	-0.68
							-0.75	-0.57
Reference	Liu, et al.[1]		Tan, et al.[2]				Gu, et al.[3]	

(B) Bimetallic surfaces

Type	Reaction	NiFe(111)			PtFe(111)		
		BE_{IS}	BE_{TS}	BE_{FS}	BE_{IS}	BE_{TS}	BE_{FS}
(c) C-H formation	$C_6H_4(OH)(OCH_3) + H \rightarrow C_6H_4H_\alpha(OH)(OCH_3)$	-0.89	0.59	-0.44	-0.63	0.54	-0.13
	$C_6H_4(OH)(OCH_3) + H \rightarrow C_6H_4H_\beta(OH)(OCH_3)$	-0.89	0.61	-0.45	-0.55	0.53	-0.12
	$C_6H_4(OH)(OCH_2) + H \rightarrow C_6H_4(OH)(OCH_3)$	-4.72	-4.13	-4.94	-4.11	-3.59	-4.24
	$C_6H_4(OCH_3) + H \rightarrow C_6H_5(OCH_3)$	-0.55	0.05	-1.12	0.99	1.48	-0.60
	$C_6H_4(OH) + H \rightarrow C_6H_5(OH)$	-0.55	-0.01	-1.22	-0.67	-0.20	-0.70
(d) O-H scission	$C_6H_4(OH)(OCH_3) \rightarrow C_6H_4(O)(OCH_3) + H$	-0.96	-0.39	-1.58	-0.50	0.44	-0.24
	$C_6H_4(OH)_2 \rightarrow C_6H_4(OH)(O) + H$	-1.09	-0.13	-1.54	-0.59	0.25	-0.83
	$C_6H_5OH \rightarrow C_6H_5O + H$	-1.22	-0.65	-1.81	-0.70	0.09	-0.81

Table S4 Bond length of C-O (*BL*, in Å), reaction energy (E_{rxn}, in eV), activation barrier (E_a, in eV) and bond dissociation energy (*BDE*, in eV) for C-O bond scission of guaiacol and its derivatives.

Type	NiFe(111)			PtFe(111)			Gas-phase	
	BL	E_{rxn}	E_a	*BL*	E_{rxn}	E_a	*BL*	*BDE*[a]
C-OH	1.39	-0.16	1.42	1.36	0.57	2.05	1.37	4.71
C-OCH_3	1.41	-0.29	1.37	1.41	0.25	1.97	1.38	4.04
O-CH_3	1.46	-0.77	0.91	1.45	-0.60	1.51	1.43	2.10
CH-OH	1.47	-1.27	0.84	1.46	-1.09	0.76		
CH-OCH_3	1.46	-1.14	0.91	1.46	-1.05	0.91		
C-O	1.34	-0.22	1.80	1.24	0.44	1.87		
O-CH_2	1.46	-0.71	0.54	1.45	-0.94	0.69		

[a]: Data was retrieved from guaiacol conversion in gas-phase.[4]

REFERENCES

1. X. Liu, W. An, C. H. Turner and D. E. Resasco, Hydrodeoxygenation of m-cresol over bimetallic NiFe alloys: Kinetics and thermodynamics insight into reaction mechanism, *J. Catal.*, 2018, **359**, 272-286.

2. Q. Tan, G. H. Wang, L. Nie, A. Dinse, C. Buda, J. Shabaker and D. E. Resasco, Different Product Distributions and Mechanistic Aspects of the Hydrodeoxygenation of m-Cresol over Platinum and Ruthenium Catalysts, *ACS Catal.*, 2015, **5**, 6271-6283.

3. G. H. Gu, C. A. Mullen, A. A. Boateng and D. G. Vlachos, Mechanism of Dehydration of Phenols on Noble Metals via First-Principles Microkinetic Modeling, *ACS Catal.*, 2016, **6**, 3047-3055.

4. A. M. Verma and N. Kishore, DFT Analyses of Reaction Pathways and Temperature Effects on various Guaiacol Conversion Reactions in Gas Phase Environment, *ChemistrySelect*, 2016, **1**, 6196-6205.